

March 2005

Numerical Modeling of Nonhomogeneous Behavior of Structured Soils during Triaxial Tests

D. S. Liyanapathirana
University of Wollongong, saml@uow.edu.au

J. P. Carter
University of Sydney

D. W. Airey
University of Sydney

Follow this and additional works at: <https://ro.uow.edu.au/engpapers>



Part of the [Engineering Commons](#)

<https://ro.uow.edu.au/engpapers/174>

Recommended Citation

Liyanapathirana, D. S.; Carter, J. P.; and Airey, D. W.: Numerical Modeling of Nonhomogeneous Behavior of Structured Soils during Triaxial Tests 2005.
<https://ro.uow.edu.au/engpapers/174>

Numerical Modeling of Nonhomogeneous Behavior of Structured Soils during Triaxial Tests

D. S. Liyanapathirana¹; J. P. Carter²; and D. W. Airey³

Abstract: The nonhomogeneous behavior of structured soils during triaxial tests has been studied using a finite element model based on the Structured Cam Clay constitutive model with Biot-type consolidation. The effect of inhomogeneities caused by the end restraint is studied by simulating drained triaxial tests for samples with a height to diameter ratio of 2. It was discovered that with the increase in degree of soil structure with respect to the same soil at the reconstituted state, the inhomogeneities caused by the end restraint will increase. By loading the sample at different strain rates and assuming different hydraulic boundary conditions, inhomogeneities caused by partial drainage were investigated. It was found that if drainage is allowed from all faces of the specimen, fully drained tests can be carried out at strain rates about ten times higher than those required when the drainage is allowed only in the vertical direction at the top and bottom of the specimen, confirming the findings of previous studies. Both end restraint and partial drainage can cause bulging of the triaxial specimen around mid-height. Inhomogeneities due to partial drainage influence the stress–strain behavior during destructuring, a characteristic feature of a structured soil. With an increase in the strain rate, the change in voids ratio during destructuration reduces, but, in contrast, the mean effective stress at which destructuration commences was found to increase. It is shown that the stress–strain behavior of the soil calculated for a triaxial specimen with inhomogeneities, based on global measurements of the triaxial response, does not represent the true constitutive behavior of the soil inside the test specimen. For most soils analyzed, the deviatoric stress based on the global measurements is about 25% less than that for the soil inside the test specimen, when the applied axial strain is about 30%. Therefore it can be concluded that the conventional global measurements of the sample response may not accurately reflect the true stress–strain behavior of a structured soil. This finding has major implications for the interpretation of laboratory triaxial tests on structured soils.

DOI: 10.1061/(ASCE)1532-3641(2005)5:1(10)

CE Database subject headings: Numerical models; Triaxial tests; Finite element method; Constitutive models; Stress distribution; Strain rate.

Introduction

Naturally occurring sedimentary and residual soil deposits are known as structured soils. The structure may arise from many different causes, but its effects on the mechanical behavior are similar (Leroueil and Vaughan 1999). Often structured soils possess bonding similar to that found in porous weak rocks. Various geological processes can cause loss of soil structure either by inducing yield (damaging the bonding or permanently rearranging the particles) or by removing bonding agents.

The mechanical behavior of a naturally occurring structured soil is different from that of the same soil when it is reconstituted in the laboratory. For example, oedometer tests carried out by Mesri et al. (1975) and Locat and Lefebvre (1985) on natural and

reconstituted clays show that the natural, structured soil usually has a higher voids ratio than a reconstituted sample of the same soil at the same stress state.

An important feature of the mechanical behavior of structured soils is the occurrence of destructuring. During this phase of behavior, the structure of the soil may be completely lost, and only a small change in stress state may cause very large strains. This phase marks the transition of the structured soil from rock-like to soil-like behavior (Lagioia and Nova 1995). Practical examples of the engineering significance of natural structure and destructuring include: the much lower than expected driving resistance of piles in carbonate soils, such as occurred at the North Rankin offshore gas production platform, Australia (King and Lodge 1988); the increase in penetration resistance due to densification of sands and silts by dynamic compaction, vibro-compaction, and blasting (Mitchell and Solymar 1984); and the subsidence induced during hydrocarbon extraction from reservoirs at Ekofisk in the North Sea (Potts et al. 1988).

The triaxial test is the most widely used test in determining the stress–strain behavior of structured soils, and the validation of constitutive models is carried out based on the behavior observed during these tests. This approach has been followed in the development of several constitutive models that have recently been used to describe the mechanical behavior of structured soils (e.g., Gens and Nova 1993; Whittle 1993; Lagioia and Nova 1995; Wheeler 1997; Kavvas and Amorosi 2000; Rouainia and Muir Wood 2000; and Liu and Carter 2002).

¹Senior Lecturer, Dept. of Civil, Mining and Environmental Engineering, Univ. of Wollongong, Wollongong, NSW, Australia 2522.

²Challis Professor, Dept. of Civil Engineering, Univ. of Sydney, Sydney, NSW, Australia 2006.

³Associate Professor, Dept. of Civil Engineering, Univ. of Sydney, Sydney, NSW, Australia 2006.

Note. Discussion open until August 1, 2005. Separate discussions must be submitted for individual papers. To extend the closing date by one month, a written request must be filed with the ASCE Managing Editor. The manuscript for this paper was submitted for review and possible publication on March 31, 2003; approved on March 5, 2004. This paper is part of the *International Journal of Geomechanics*, Vol. 5, No. 1, March 1, 2005. ©ASCE, ISSN 1532-3641/2005/1-10-23/\$25.00.

Ideally, the stresses and strains inside a triaxial specimen should be uniform. However, during laboratory testing the smoothness of the contact between the sample and the end platens, the height to diameter ratio, the hydraulic boundary conditions, and the rate of loading all influence the observed stress-strain behavior. They may cause the observed response to deviate from the ideal situation and subsequently the global measures of stresses and strains may not represent the true soil behavior occurring inside the triaxial specimen.

Several numerical studies based on the finite element method have been carried out to study the effect of nonuniform behavior during triaxial testing on the measured stress-strain behavior of reconstituted soils. Some of these studies adopted the Modified Cam Clay model (e.g., Carter 1982; Airey 1991; and Sheng et al. 1997) while others assumed linear-elastic-perfectly-plastic models (e.g., Schanz and Gussman 1994). Predictions of the values of shear, radial, and tangential stresses vary depending on how well the boundary conditions have been satisfied. Balla (1960) studied the nonuniformities caused by end restraint by deriving stress-strain relationships based on the theory of elasticity. A feature that is common to all elastic solutions found in the literature is the unrealistically high concentration of contact stresses at the edges of the specimen (Saada and Townsend 1981).

Generally, triaxial tests are carried out on specimens with a height to diameter ratio of about 2. Over the years several researchers have concluded that this height to diameter ratio is sufficient to eliminate or reduce to an insignificant level any effects of inhomogeneities caused by the end restraint. According to Lee (1978), the experimental work by Taylor in 1941 led to the conclusion that reliable results could be obtained with height to diameter ratios in the range of 1.5–3. Bishop and Green (1965) and Duncan and Dunlop (1968) carried out triaxial tests with lubricated and nonlubricated end platens and showed that the reduction of end restraint by lubrication has no significant effect on the observed strength of the triaxial specimen if the samples have the usual height to diameter ratio of 2 or more. Schanz and Gussmann (1994) carried out finite element simulations and also concluded that the sample geometry does not have any significant influence on the shear strength measured during triaxial testing if the height to diameter ratio is greater than or equal to 2.

In this paper, attention is focused on the influence of nonuniform behavior of test samples of structured soils due to end restraint and insufficient drainage during so-called “drained” triaxial shearing. Triaxial specimens with a height to diameter ratio of 2 have been simulated using the Structured Cam Clay model developed by Liu and Carter (2002).

Numerical Procedure

The stress-strain behavior during the destructuring phase and the volumetric characteristics of a triaxial specimen subject to different end and drainage conditions have been simulated using an axisymmetric finite element model. The initial conditions in each of the models corresponded to the end of isotropic consolidation. The simulations were carried out by incorporating the Structured Cam Clay model (Liu and Carter 2002) with Biot-type consolidation (Small et al. 1976) into the finite element program AFENA (Carter and Balaam 1995) developed at the Univ. of Sydney.

The finite element mesh used for the analysis of triaxial specimens is shown in Fig. 1. Each specimen has been discretized into 100 eight-noded axisymmetric quadrilateral elements with three nodal degrees of freedom, two displacement components, and the

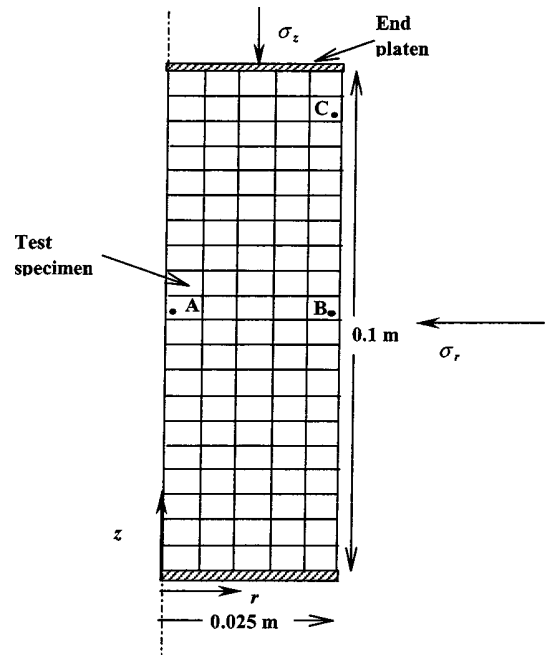


Fig. 1. Finite element mesh used for analysis of triaxial specimen

pore-water pressure. The node spacing in both radial and vertical directions is 0.005 m. The radius of each triaxial specimen was 0.025 m and the height was 0.1 m.

Constitutive Model

The soil was modeled using the Structured Cam Clay model (Liu and Carter 2002). The basis for this model is the Modified Cam Clay model developed by Roscoe and Burland (1968). Similar to the Modified Cam Clay model, the yield surface of the structured soil in p' - q space is elliptical, passes through the origin of stress space, and has the same shape for the yield surface as the reconstituted soil. In this model, the parameters controlling elastic deformation of structured soil are assumed to be the same as those of the soil after it has been reconstituted.

In the Structured Cam Clay model, three additional parameters have been introduced to capture the effects of structure. They are, namely, the destructuring index b , the additional voids ratio sustained by the structured soil when virgin yielding begins Δe_i , and another parameter ω , to describe the influence of soil structure on the plastic flow rule. In what follows, all properties of reconstituted soil are denoted by the superscript *.

The yield surface of the soil depends on the stress state and the plastic volumetric strain, given by

$$F = q^2 + M^{*2}p'(p' - p'_c) \quad (1)$$

where p' = mean effective stress; p'_c = size of the current yield surface; q = deviatoric stress; and M^* = friction parameter of the reconstituted soil that controls the aspect ratio of the yield locus. Hence an incremental change in the yield function is given by

$$dF = \left\{ \frac{\partial F}{\partial \sigma'} \right\}^T \{d\sigma'\} + \frac{\partial F}{\partial \varepsilon_v^p} d\varepsilon_v^p \quad (2)$$

where $d\varepsilon_v^p$ = increment in plastic volumetric strain and $\{d\sigma'\}$ = corresponding increment in the stress state of the soil. Since the problem is axisymmetric, $\{d\sigma'\}$ is given by

$$\{d\sigma'\} = \begin{Bmatrix} d\sigma'_r \\ d\sigma'_z \\ d\sigma'_\theta \\ d\tau_{rz} \end{Bmatrix} \quad (3)$$

where $d\sigma'_r$, $d\sigma'_z$, and $d\sigma'_\theta$ =respectively, radial, vertical, and tangential components of the effective stress increment and, $d\tau_{rz}$ =increment in shear stress.

Although strains will contain both elastic and plastic components, only elastic strains can generate stresses through the elastic constitutive matrix $[D]$. Therefore, the change in stress state is given by

$$\{d\sigma'\} = [D]\{\{d\varepsilon\} - \{d\varepsilon^p\}\} = ([D] - [D_p])\{d\varepsilon\} \quad (4)$$

where $[D_p]$ =plastic constitutive matrix; $\{d\varepsilon\}$ =increment in total strains; and $\{d\varepsilon^p\}$ =increment in plastic strains which is given by

$$\{d\varepsilon^p\} = \lambda \begin{Bmatrix} \partial G \\ \partial \sigma' \end{Bmatrix} \quad (5)$$

where λ =plastic scaling factor and G =plastic potential function. For the Structured Cam Clay model, nonassociated plastic flow is assumed. Therefore, the plastic potential G is different from the flow rule F . By substituting Eqs. (4) and (5) into (2), the plastic scaling factor can be obtained as

$$\lambda = \frac{\begin{Bmatrix} \partial F \\ \partial \sigma' \end{Bmatrix}^T [D] \{d\varepsilon\}}{\begin{Bmatrix} \partial F \\ \partial \sigma' \end{Bmatrix}^T [D] \begin{Bmatrix} \partial G \\ \partial \sigma' \end{Bmatrix} - \frac{\partial F}{\partial \varepsilon_v^p} \frac{\partial G}{\partial \sigma'}} \quad (6)$$

From Eq. (4), the plastic constitutive matrix $[D_p]$ can be obtained as

$$[D_p] = \frac{[D] \begin{Bmatrix} \partial G \\ \partial \sigma' \end{Bmatrix} \begin{Bmatrix} \partial F \\ \partial \sigma' \end{Bmatrix}^T [D]}{\begin{Bmatrix} \partial F \\ \partial \sigma' \end{Bmatrix}^T [D] \begin{Bmatrix} \partial G \\ \partial \sigma' \end{Bmatrix} - \frac{\partial F}{\partial \varepsilon_v^p} \frac{\partial G}{\partial \sigma'}} \quad (7)$$

To obtain the plastic constitutive matrix $[D_p]$ for the structured soil, the vectors $\{\partial F/\partial \sigma'\}$, $\{\partial G/\partial \sigma'\}$, and the scalars $\partial G/\partial \sigma'$, and $\partial F/\partial \varepsilon_v^p$ should be substituted in Eq. (7). Explicit expressions for these quantities are presented below.

An increment in the plastic volumetric strain $d\varepsilon_v^p$ can only occur with a change in the current yield surface controlled by p'_c . Hence, the scalar $\partial F/\partial \varepsilon_v^p$ can be written as

$$\frac{\partial F}{\partial \varepsilon_v^p} = \frac{\partial F}{\partial p'_c} \frac{\partial p'_c}{\partial \varepsilon_v^p} \quad (8)$$

According to Liu and Carter (2002), an increment in plastic volumetric strain of a structured soil is given by

$$d\varepsilon_v^p = (\lambda^* - \kappa^*) \frac{dp'_c}{(1+e)p'_c} + b\Delta e \left(1 + \frac{\eta}{M^* - \eta}\right) \frac{dp'_c}{(1+e)p'_c} \quad (9)$$

where η =ratio between deviatoric stress and mean effective stress; λ^* and κ^* =respectively, gradients of normal compression and, unloading and reloading lines of the reconstituted soil in $e-\ln(p')$ space; e =voids ratio of the structured soil; and Δe =difference in voids ratio between the structured intact soil and the corresponding reconstituted soil at the same stress state. By

studying different structured soils, Liu and Carter (2002) suggested that the destructuring index b usually varies between 1 and 30.

Substituting Eq. (9) and $\partial F/\partial p'_c$ from Eq. (1) into Eq. (8) provides

$$\frac{\partial F}{\partial \varepsilon_v^p} = \frac{(-M^{*2}p')(1+e)p'_c}{\left((\lambda^* - \kappa^*) + b\Delta e \left(1 + \frac{\eta}{M^* - \eta}\right)\right)} \quad (10)$$

The yield function F is known and so the vector $\{\partial F/\partial \sigma'\}$ can be calculated from

$$\left\{ \frac{\partial F}{\partial \sigma'} \right\} = \begin{Bmatrix} \frac{\partial F}{\partial p'} \frac{\partial p'}{\partial \sigma'_r} + \frac{\partial F}{\partial q} \frac{\partial q}{\partial \sigma'_r} \\ \frac{\partial F}{\partial p'} \frac{\partial p'}{\partial \sigma'_z} + \frac{\partial F}{\partial q} \frac{\partial q}{\partial \sigma'_z} \\ \frac{\partial F}{\partial p'} \frac{\partial p'}{\partial \sigma'_\theta} + \frac{\partial F}{\partial q} \frac{\partial q}{\partial \sigma'_\theta} \\ \frac{\partial F}{\partial q} \frac{\partial q}{\partial \tau_{rz}} \end{Bmatrix} \quad (11)$$

where

$$p' = \frac{(\sigma'_r + \sigma'_z + \sigma'_\theta)}{3} \quad (12)$$

and

$$q = \frac{1}{\sqrt{2}} \left((\sigma'_r - \sigma'_z)^2 + (\sigma'_z - \sigma'_\theta)^2 + (\sigma'_\theta - \sigma'_r)^2 + 6\tau_{rz}^2 \right)^{1/2} \quad (13)$$

The vector $\{\partial G/\partial \sigma'\}$ can be obtained by substituting the plastic potential function G instead of the yield function F in Eq. (11). The scalar quantity $\partial G/\partial \sigma'$ is given by

$$\frac{\partial G}{\partial \sigma'} = \frac{\partial G}{\partial p'} \left(\frac{\partial p'}{\partial \sigma'_r} + \frac{\partial p'}{\partial \sigma'_z} + \frac{\partial p'}{\partial \sigma'_\theta} \right) + \frac{\partial G}{\partial q} \left(\frac{\partial q}{\partial \sigma'_r} + \frac{\partial q}{\partial \sigma'_z} + \frac{\partial q}{\partial \sigma'_\theta} \right) \quad (14a)$$

$$\frac{\partial q}{\partial \sigma'_r} = \frac{2\sigma'_r - \sigma'_z - \sigma'_\theta}{2q} \quad (14b)$$

$$\frac{\partial q}{\partial \sigma'_z} = \frac{2\sigma'_z - \sigma'_r - \sigma'_\theta}{2q} \quad (14c)$$

$$\frac{\partial q}{\partial \sigma'_\theta} = \frac{2\sigma'_\theta - \sigma'_r - \sigma'_z}{2q} \quad (14d)$$

According to Eqs. (14b), (14c), and (14d), irrespective of G , the second term in Eq. (14a) is zero. Although G may be unknown, $\partial G/\partial p'$ and $\partial G/\partial q$ are known and proportional to, respectively, the increment in plastic volumetric strain $d\varepsilon_v^p$ given by Eq. (9) and the increment in plastic deviatoric strain $d\varepsilon_d^p$ given by Liu and Carter (2002)

$$d\varepsilon_d^p = 2(1 - \omega\Delta e) \left[(\lambda^* - \kappa^*) \pm b\Delta e \left(\frac{M^*}{M^* - \eta} \right) \right] \times \frac{\eta}{(M^{*2} - \eta^2)} \left(\frac{dp'_c}{(1+e)p'_c} \right) \quad (15)$$

The negative sign in Eq. (15) is used only when soil reaches the yield surface with $\eta > M^*$, where softening occurs. During the

softening process, soil structure is broken down and the yield surface shrinks until the soil reaches a critical state of deformation with the current stress state always remaining on the yield surface. Therefore, stresses can reduce during the process of destructuring. Conversely, if the soil reaches the yield surface with $\eta < M^*$, stresses can increase during the destructuring process. In both cases the rate of increase or decrease of stress with respect to the change in voids ratio depends on the destructuring index b . Normally for soils with higher values of destructuring index, destructuring occurs with very little or no change in stress.

The change in voids ratio of structured soils along a general stress path in $e-\ln(p')$ space is assumed (Liu and Carter 2002) to follow

$$e = e^* + \Delta e_i \left(\frac{p'_{c0}}{p'_c} \right)^b \quad \text{for } p'_c \geq p'_{c0} \quad (16)$$

where p'_c = size of the current yield surface; and Δe_i = initial additional void ratio.

Global Measurements

The local stress paths and stress-strain curves at selected points within the specimen are compared with global measures of stresses and strains, similar to laboratory measurements. The global axial stress σ_a is the total force applied on the end platen divided by the cross-sectional area of the volumetrically equivalent right cylinder. The global radial stress σ_r is equal to the applied cell pressure.

During drained triaxial testing and in the absence of backpressure, σ_a and σ_r are equivalent to the global effective axial stress σ'_a and global effective radial stress σ'_r . The global deviatoric stress is $q = \sigma'_a - \sigma'_r$ and the global mean effective stress is $p' = (\sigma'_a + 2\sigma'_r)/3$. The global axial strain ϵ_a is equal to the vertical displacement of the top platen divided by the initial height of the specimen. The global radial strain ϵ_r is the average radial displacement of the specimen, based on the volumetrically equivalent right cylinder, divided by the initial radius of the specimen.

Material Properties

Numerical simulations have been conducted for an ideal material with parameter values selected as being representative of natural calcarenite (Lagioia and Nova 1995) and Corinth Canal Marl (Anagnostopoulos et al. 1991). These materials have been selected because the Natural Calcarenite has a very high destructuring index and the Corinth Canal Marl has a relatively low destructuring index. Because of this choice it is possible to examine the extremes of structured soil behavior. The complete set of properties for these two soils is given in Table 1.

The value of M^* was determined from the experimental yield loci for each material in $p'-q$ space. Using the $e-\ln(p')$ curve for the intact soil subject to isotropic compression κ^* , Δe_i and p'_{c0} were obtained. The value of λ^* was obtained from the $e-\ln(p')$ curve for the fully destructured soil. The value of the model parameter ω lies between 0 and $1/\Delta e_i$ (Liu and Carter 2002). Thus $\omega \Delta e_i$ was set to 0.5, so that a mid-range value was obtained for ω . The value of destructuring index b was determined by simulating the isotropic compression behavior of each soil.

Before investigating the influence of inhomogeneities in the triaxial specimen on destructuring and the stress-strain behavior, it is important to investigate whether the experimentally observed behavior of structured soils can be obtained from the numerical

Table 1. Values of Model Parameters for Natural Calcarenite and Corinth Canal Marl

Parameter	Natural Calcarenite (Lagioia and Nova 1995)	Corinth Canal Marl (Anagnostopoulos et al. 1991)
M^*	1.45	1.38
λ^*	0.2164	0.039
κ^*	0.0136	0.008
b	30.0	0.4
Δe_i	0.15	0.1
ω	3.33	4.9
P'_{c0} (kPa)	2,400	3,800
e^*_{cs}	2.5	0.725
ν^*	0.13	0.25

procedure described previously. In determining parameters for Natural Calcarenite and Corinth Canal Marl, it has been assumed that the stresses and strains inside the samples are uniform but in reality, it is very unlikely that the stresses and strains were uniform during the physical experiments, in which case the parameters selected for the numerical simulations are affected by end-restraining effects.

Figs. 2(a and b) show, respectively, the isotropic compression behavior of Natural Calcarenite with a destructuring index of 30 and Corinth Canal Marl with a destructuring index of 0.4. It can be seen that the numerical simulations are able to reproduce the experimental data quite well. For soils with very high destructur-

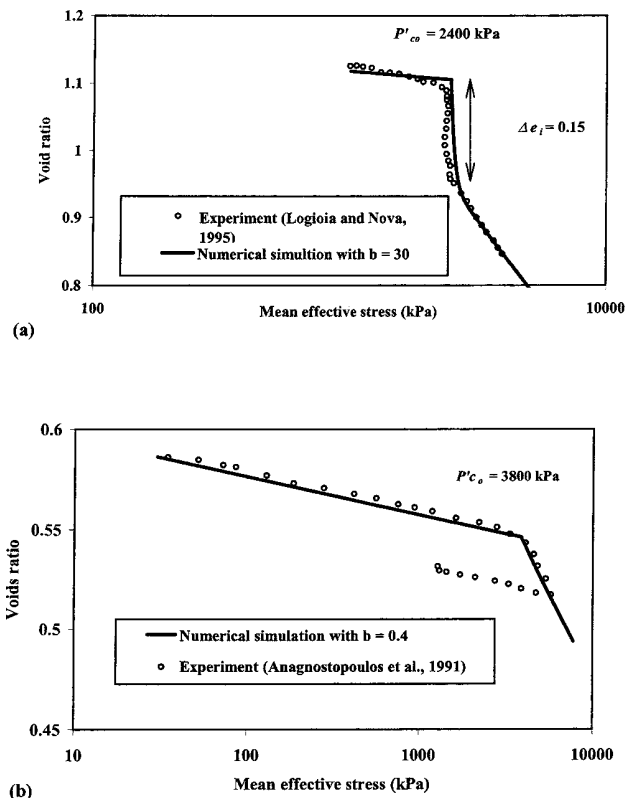


Fig. 2. (a) Numerical simulation of isotropic compression test for Natural Calcarenite (destructuring index, $b=30$) and (b) numerical simulation of isotropic compression test for Corinth Canal Marl (destructuring index, $b=0.4$)

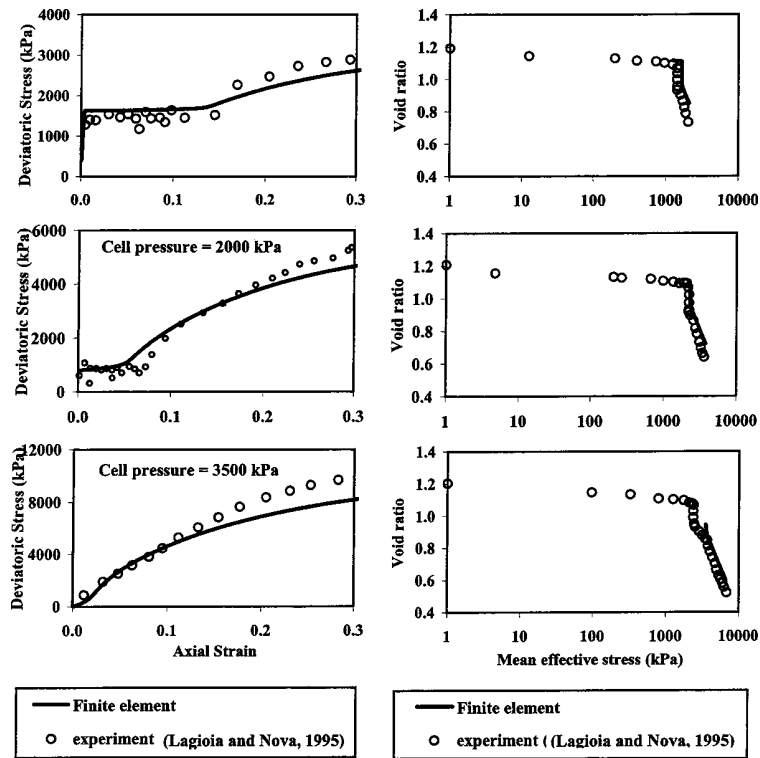


Fig. 3. Comparison of finite element simulations with experiments by Lagioia and Nova (1995) for Natural Calcarenite

ing index, such as the natural calcarenite, there is a clear destructuring phase during which the change in stress is negligible.

Drained compression tests were simulated for the natural calcarenite with constant cell pressures of 1,100, 2,000, and 3,500 kPa, and in each case with the initial conditions corresponding to the end of the consolidation phase. Figs. 3(a and b) show, respectively, the variation in deviatoric stress with axial strain and the variation of voids ratio with mean effective stress. It can be seen that for the tests with cell pressures of 1,100 and 2,000 kPa, destructuring in the experiments of Lagioia and Nova (1995) takes place at constant stress, and this is reproduced by the high destructuring index ($b=30$) used to represent Natural Cal-

carenite. A distinct destructuring phase cannot be seen during drained shearing for the test at a cell pressure of 3,500 kPa because the initial stress is much larger than the stress at which destructuring commences during isotropic compression of the specimen, i.e., 2,400 kPa. Since this soil has a very high destructuring index, the model predicts that the structure of the soil will have been completely destroyed by this cell pressure, as indicated by Eq. (16). During shearing its behavior is similar to the reconstituted soil at the same stress state.

Fig. 4 shows the variation of deviatoric stress with axial strain predicted for a triaxial specimen of Corinth Canal Marl, which has a very low destructuring index ($b=0.4$). The experimental

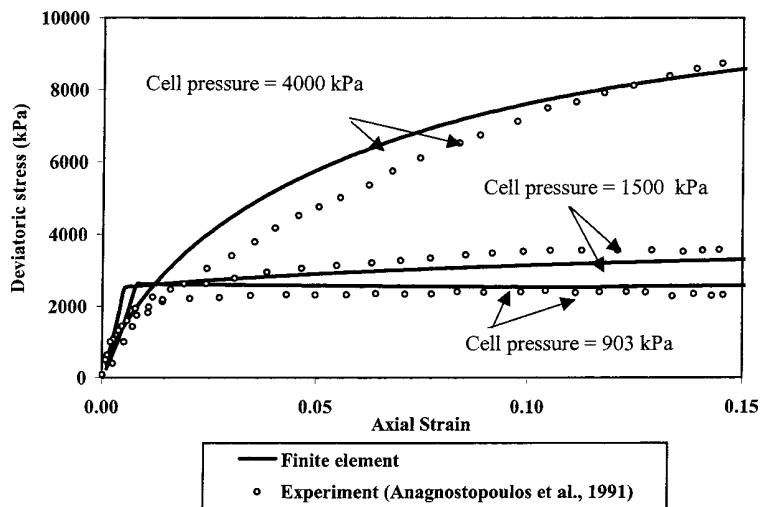


Fig. 4. Comparison of finite element simulations with experiments by Anagnostopoulos et al. (1991) for Corinth Canal Marl

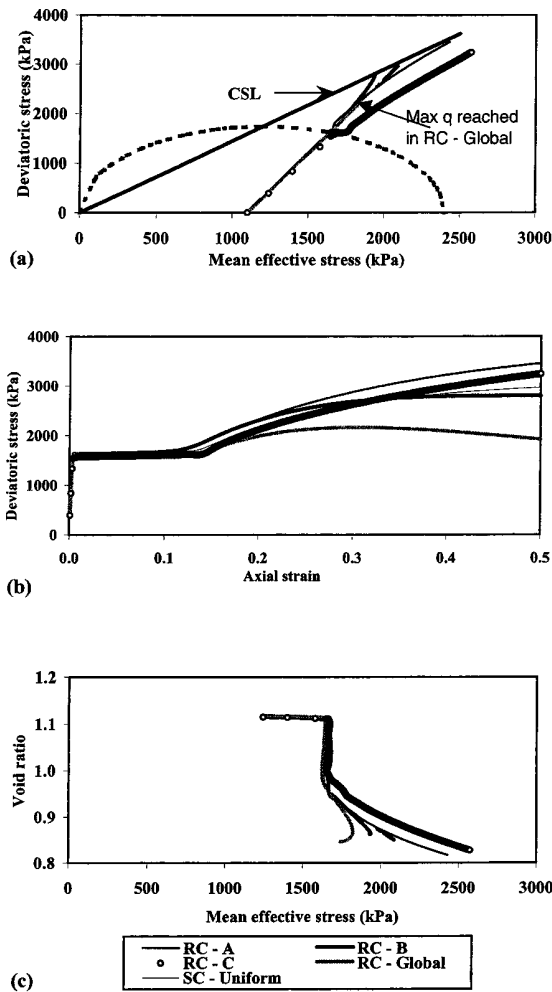


Fig. 5. (a) Stress paths in p' - q plane for Natural Calcarenite; (b) variation of deviatoric stress with axial strain for Natural Calcarenite; and (c) variation of void ratio with mean effective stress for Natural Calcarenite

data for Corinth Canal Marl given by Anagnostopoulos et al. (1991) are also shown in Fig. 4. It can be seen that during destructuring the stresses increase with increase in strain, but a distinct destructuring phase cannot be seen, in contrast to the calcarenite with high destructuring index.

From the study described above it can be seen that the Structured Cam Clay model can simulate the experimentally observed behavior of both Natural Calcarenite and Corinth Canal Marl, two different but structured soils. In the following sections, description is provided of the use of the Structured Cam Clay model to study the effect of inhomogeneities in the triaxial specimen on the global and local stress-strain behavior.

Effects of End Restraint

In order to study the effects of end restraint during drained triaxial tests, stresses and strains obtained for the ideal case with perfectly smooth end contact, where there is no friction at the interface between the specimen and the end platens, are compared with those for the case with completely rough contact, where no sliding is allowed at the interface between the specimen and the end

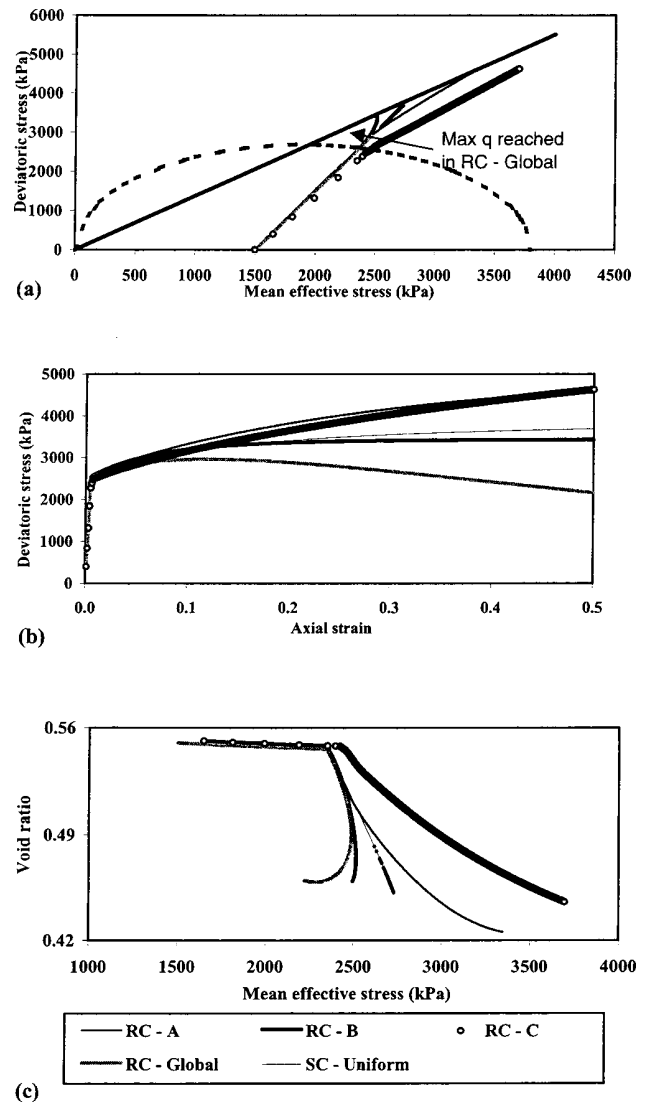


Fig. 6. (a) Stress paths in p' - q plane for Corinth Canal Marl; (b) variation of deviatoric stress with axial strain for Corinth Canal Marl; and (c) variation of void ratio with mean effective stress for Corinth Canal Marl

platens. It is well known that during triaxial tests on sand, severe nonuniformities in strain can develop, even under negligibly small end restraint, and this can have a significant influence on the measured shear strength and the stress-strain characteristics of the sand (e.g., Balasubramaniam 1976; Lade 1982).

Conditions similar to the rough contact may occur when the end platens, with the same diameter as the specimen, are sealed to the specimen using a rubber membrane (Sheng et al. 1997). Although a perfectly smooth contact is unlikely to be achieved, it has been demonstrated that adequately uniform conditions can be achieved by using enlarged lubricated end platens. These are the two extreme conditions of soil-platen interaction considered in the present study. For these conditions, stresses, strains, and destructuring within the specimen are compared for both the Natural Calcarenite and Corinth Canal Marl during triaxial testing under cell pressures of 1,100 and 1,500 kPa, respectively. Due to the difference in their destructuring index, these two soil types be-

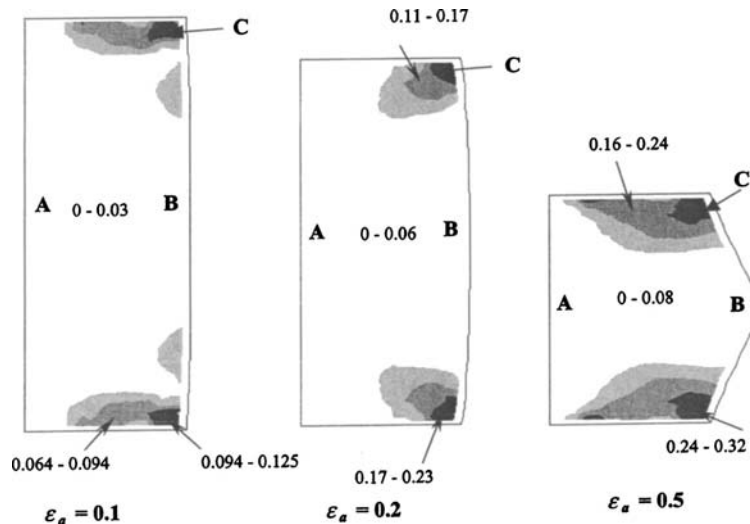


Fig. 7. Distribution of principal stress ratio $(\sigma_2 - \sigma_3) / (\sigma_1 - \sigma_3)$ inside triaxial specimen

have differently during triaxial testing, and represent reasonable bounds on real behavior.

For the case of smooth contact, the stresses and strains are uniform throughout the sample. For the case with rough contact, inhomogeneities in the sample are studied by comparing stresses and changes in voids ratio at Points A, B, and C shown in Fig. 1. Points A and B represent the mid-region of the sample and Point C represents the soil behavior closer to the end platens. Values based on the global measurements are also shown in these figures.

Inhomogeneities in Natural Calcarene and Corinth Canal Marl samples

When the stress state remains inside the initial yield surface, the stress paths for Points A, B, C and the path based on global measurements coincide with each other, as can be seen in Figs. 5(a) and 6(a). This indicates that the inhomogeneities in the sample are not significant until the beginning of plastic deformations inside the triaxial specimen, and conventional global measurements should be able to identify the start of the destructuring phase. Since destructuring starts when the stress state reaches the initial yield surface, significant inhomogeneities in the specimen develop only after yielding and destructuring commence.

If the order of yielding inside the specimen is examined, it can be seen that the destructuring process (which physically probably corresponds to crushing of the calcareous particles and breakage of the interparticle bonds) commences at the mid-region of the specimen. Point C, which is adjacent to the end platens, reaches the yield surface while destructuring continues in the mid-region. Hence, a constant deviatoric stress is observed just after destructuring commences, while the mean effective stress increases, i.e., local softening is observed at Point C of the Natural Calcarene specimen. This can be seen in Fig. 5(a). According to Fig. 6(a), for the Corinth Canal Marl local softening cannot be detected at Point C owing to the slow destructuring process taking place inside the triaxial specimen.

According to Figs. 5(a) and 6(a), the stress paths based on the global measurements do not reach the critical state line. Both deviatoric and mean effective stresses increase up to a certain point, but after that, while local stresses increase, the global stresses start to decrease with the increase in applied axial strain.

Behavior similar to this has been observed by Sheng et al. (1997) in numerical studies carried out using the Modified Cam Clay model. The reason is that the calculated global stresses are affected by the deformation pattern of the triaxial specimen as well as by the constitutive law of the material.

Points A, B, and C of the specimen with rough contact take different stress paths in the p' - q space and they are different to the ideal stress path taken when the contact between the end platens and the specimen are smooth. The stress path at B reaches the critical state first in the specimen with rough contact, at lower values of p' and q compared to the stress path followed by the specimen with smooth contact. The stress path at Point A reaches the critical state line at higher values of p' and q compared to the stress path followed by the specimen with smooth contact. The stress path at C does not appear to reach the critical state line but it moves up, i.e., hardens, along a stress path approximately parallel to the critical state line.

When using the Structured Cam Clay model, similar to the Modified Cam Clay model, stress states in an ideal triaxial specimen exhibiting completely uniform behavior can reach critical state conditions only under triaxial compression conditions ($\sigma_2 = \sigma_3$), where σ_2 and σ_3 are intermediate and minor principal stresses, respectively (Gens and Potts 1988). Fig. 7 shows the variation of $(\sigma_2 - \sigma_3) / (\sigma_1 - \sigma_3)$ inside the triaxial specimen at 10, 20, and 50% axial strain. At Points A and B the principal stress ratio is nearly zero and the stress paths reach the critical state line,

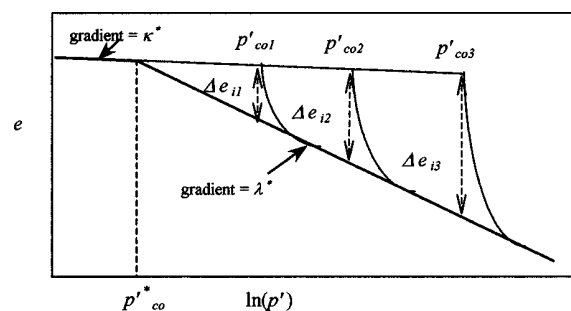


Fig. 8. Variation of p'_{co} with Δe_i for structured soil

Table 2. Variation of Inhomogeneity with Additional Void Ratio Sustained by Structured Soil at 20% Axial Strain ($b=30$)

Additional void ratio Δe_i	Mean effective stress, p' (MPa)			Deviatoric stress, q (MPa)		
	Smooth	Rough	% difference	Smooth	Rough	% difference
0 (reconst.)	1.9	1.83	3.7	2.39	2.2	8.0
0.15	1.83	1.76	3.8	2.18	1.99	8.7
0.2	1.85	1.73	6.5	2.24	1.88	16.1
0.25	2.04	1.89	7.4	2.82	2.37	16.0

but at Point C, near the rough ends, it increases significantly above zero. This may have contributed to the observed behavior of the stress path at Point C.

Figs. 5(b) and 6(b) show the variation of deviatoric stress with applied axial strain for Natural Calcarenite and Corinth Canal Marl, respectively. For structured soils with a high destructuring index, such as the Natural Calcarenite, the stresses remain constant during the destructuring process. For structured soils with a low destructuring index, such as the Corinth Canal Marl, the stresses increase with an increase in applied axial strain even during the destructuring process. The deviatoric stresses based on the global measurements are much lower than the local deviatoric stresses. Although the deviatoric stress increases locally, the global deviatoric stress starts to decrease when the applied axial strain exceeds about 0.3. Global deviatoric stresses obtained for the cases with rough contact are about 65 and 60% of those given by the case with smooth contact for the Natural Calcarenite and Corinth Canal Marl, respectively, when the applied axial strain is 0.5. These global trends are similar to the trends observed by Sheng et al. (1997) in the response of Norrköping clay predicted using the Modified Cam Clay model.

Figs. 5(c) and 6(c) show the variation of voids ratio with the mean effective stress. For Natural Calcarenite, a clear destructuring phase is marked by the sudden drop in the voids ratio at a constant mean effective stress, unlike the Corinth Canal Marl where this is not evident. After destructuring, the soil structure has been completely removed and it behaves as reconstituted soil and starts to harden. In Fig. 5(c), hardening starts at Point B when the voids ratio is 0.94 similar to the case with smooth contact. Gradually, hardening continues and the zone of hardening grows towards the center of the specimen and towards the end platens. At Points A and C, hardening starts at voids ratios of 0.97 and 0.99, respectively. For Corinth Canal Marl, hardening occurs during the destructuring. This behavior is observed for many structured clays during triaxial testing. According to Figs. 6(b and c), Point B hardens at a slower rate than Points A and C. This may be due to the bulging of the sample at mid-height, adjacent to the outer boundary. Although the voids ratio changes based on the global measurements for the cases with rough contact agree well

with the voids ratio changes observed for the cases with the smooth contact, the changes in mean effective stress are different.

During hardening, inhomogeneities in the triaxial specimen become significant as shown in Figs. 5(a–c) and 6(a–c). The influence of end restraint on inhomogeneities is more significant for Corinth Canal Marl than for Natural Calcarenite. This indicates that the degree of inhomogeneity in the sample is a function of the structural properties of the soil.

Influence of Structural Properties of Soil on Degree on Inhomogeneity

In order to study the influence of structural properties of the soil on the degree of inhomogeneity, values of p' and q obtained with smooth end platens have been compared with the global values of p' and q obtained with rough end platens.

For structured soils, p'_{c_0} , the size of the yield surface of the structured soil is always greater than $p'_{c_0}^*$, the size of the yield surface of the same soil at the reconstituted state. The relation between these parameters depends on the additional void ratio sustained by the soil structure Δe_i as illustrated in Fig. 8, and is assumed to be given by

$$p'_{c_0} = p'_{c_0}^* \exp\left(\frac{\Delta e_i}{\lambda^* - \kappa^*}\right) \quad (17)$$

It was found that the influence of ω , which describes the influence of soil structure on the plastic potential of the soil, on the inhomogeneity of the sample was not significant. Therefore, only the effects of the destructuring index b and the additional void ratio Δe_i have been studied. Tables 2 and 3 summarize the results obtained from varying Δe_i and b , respectively, when the applied axial strain is 20%. The percentage difference in the values of p' and q obtained from the smooth and rough platens gives an indication of the degree of inhomogeneity inside the sample.

It can be seen from Table 2 that an increase in the degree of structure, achieved by increasing Δe_i , leads to the influence of the stress inhomogeneities becoming more significant. However, Table 3 shows that as the destructuring index increases, the influ-

Table 3. Variation of Inhomogeneity with Destructuring Index at 20% Axial Strain ($\Delta e_i=0.15$)

Destructuring index, b	Mean effective stress, p' (MPa)			Deviatoric stress, q (MPa)		
	Smooth	Rough	% difference	Smooth	Rough	% difference
0.1	2.02	1.90	5.9	2.75	2.39	13.0
0.25	1.97	1.86	5.6	2.6	2.27	12.7
1	1.87	1.79	4.3	2.32	2.06	11.2
30	1.83	1.76	3.8	2.18	1.99	8.7

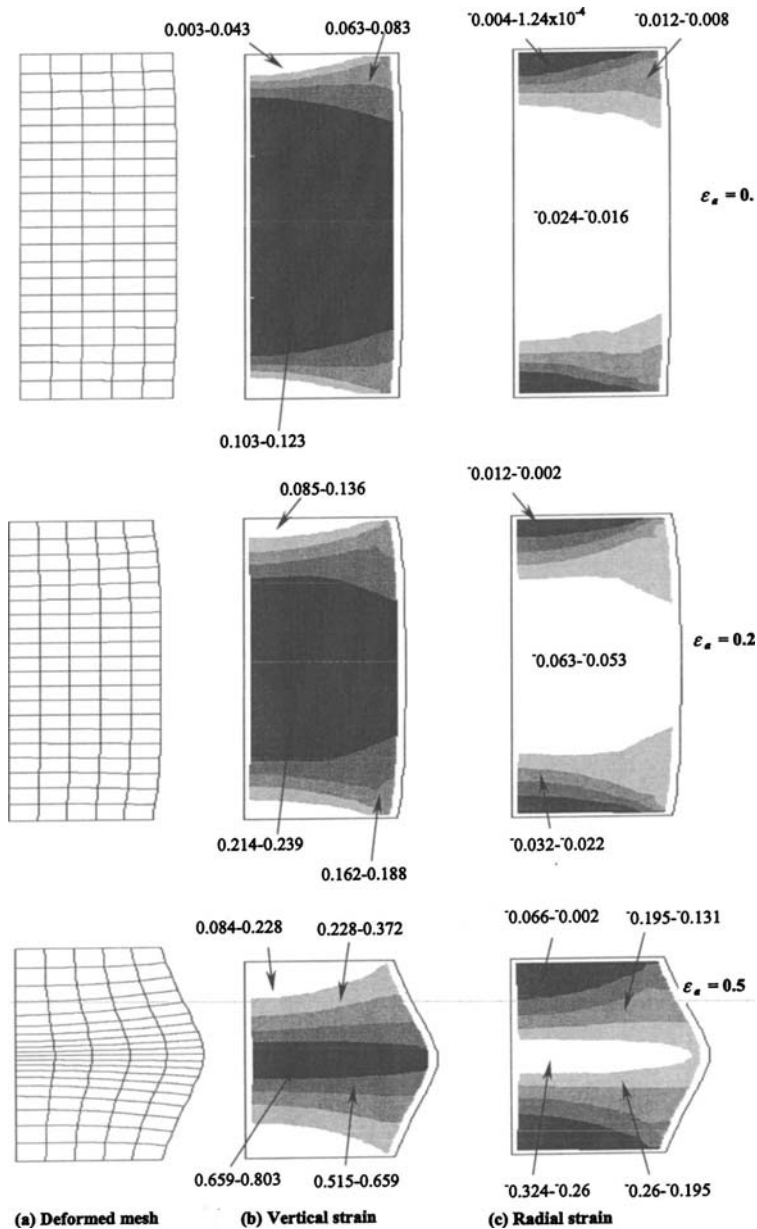


Fig. 9. Deformed finite element mesh and vertical and radial strain distributions inside specimen of Natural Calcarene when applied axial strain is 10, 20, and 50%

ence of the inhomogeneities becomes less significant. When $b = 30$, destructuring occurs rapidly with no change in stress and by 20% axial strain the soil has lost any effects of its initial structure. For soils with low destructuring indices, destructuring occurs slowly and they still possess some structure at 20% axial strain. Thus it appears that a rapid collapse of soil structure leads to minimization of the effects of stress and strain inhomogeneities, and provided Δe_i is low the inhomogeneities may be no worse than when testing reconstituted soils. As a result, the triaxial testing of soils with a high destructuring index and low Δe_i is potentially more accurate than testing soils with a low destructuring index and high Δe_i . In all cases the stress-strain behavior based on global measures does not represent the true material behavior inside the triaxial specimen.

Stress and Strain Distributions Inside Triaxial Specimen

Although inhomogeneities are more significant for Corinth Canal Marl, a clear destructuring phase is not observed for this material. Therefore, in order to study in more detail the stress and strain distributions inside the triaxial specimen, the Natural Calcarene specimen has been selected.

Fig. 9(a) shows the deformed finite element mesh during destructuring ($\epsilon_a = 0.1$), just after destructuring ($\epsilon_a = 0.2$), and at the end of loading ($\epsilon_a = 0.5$) for the case with rough contact. Due to the end restraint, lateral strains are retarded near the end platens. Therefore, the sample starts to bulge gradually at the center with

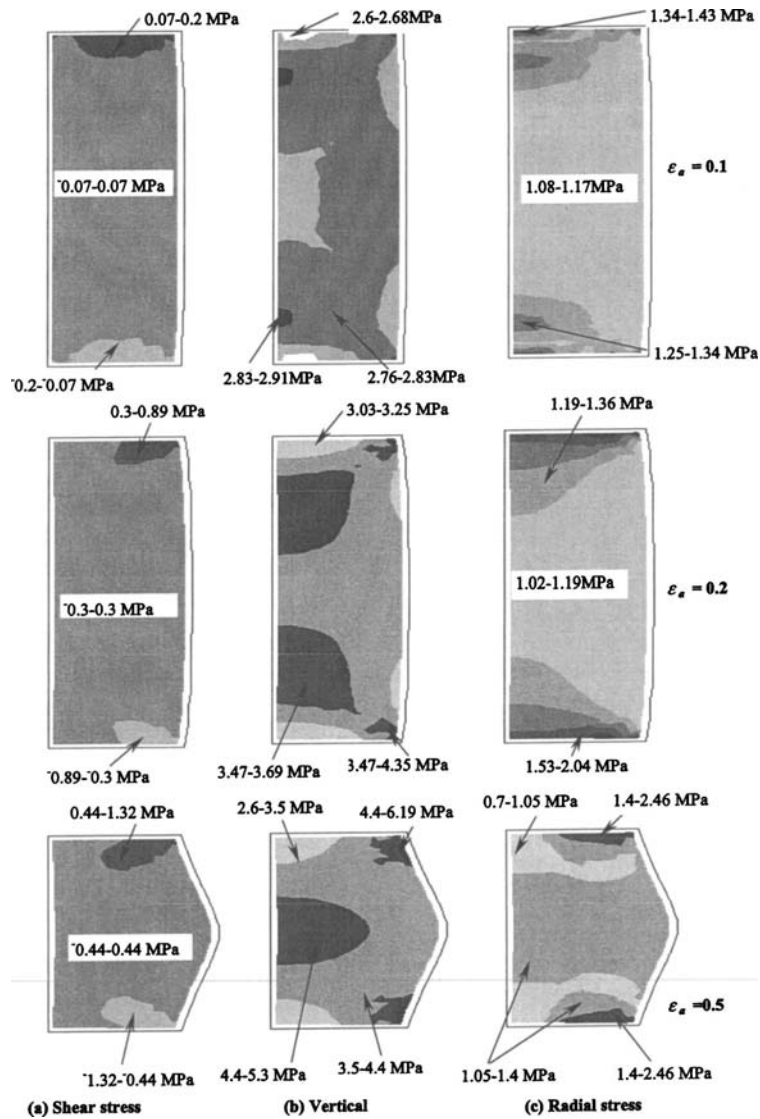


Fig. 10. Shear, vertical, and radial stress distributions inside specimen of Natural Calcarene when applied axial strain is 10, 20, and 50%

the increase in applied axial strain. Figs. 9(b and c) show, respectively, the distributions of vertical and radial strains within the sample. When the applied axial strain is 0.1, for the case with smooth contact, the vertical and radial strains are, respectively, 0.1 and -0.033 . For the case with rough contact, the vertical strain varies between 0.003 and 0.123, and the radial strain varies between -0.024 and nearly zero adjacent to the center of the end platen. It can be seen that the inhomogeneities increase with the increase in loading.

When the applied axial strain is 0.5, for the case with smooth contact, throughout the specimen the axial and radial strains are 0.5 and -0.183 , respectively, at the end of loading. For the rough contact, the distribution of strains is highly nonuniform. The axial strain varies between 0.084 and 0.803, and the radial strain varies between -0.002 and -0.324 . The highest axial compression and the highest radial extension are experienced at the center of the specimen.

The shear stresses induced at the ends are reduced towards the center of the sample giving zero shear stresses at the mid-height. This can be clearly seen in Fig. 10(a), which shows the shear stress distribution inside the specimen when the applied axial

strain is 0.1, 0.2, and 0.5. Hence, the vertical and radial stresses become the principal stresses. Throughout the loading, the highest stresses are developed closer to the edges of the end platens. With increasing axial strain, stresses develop from the edges of the end platens into the specimen in an X shape. Figs. 10(b and c) show, respectively, the vertical and radial stress distributions inside the specimen. For the smooth contact, when the axial strain is 0.5, the uniform vertical and radial stresses inside the specimen are 4,064 and 1,100 kPa, respectively. For the rough contact, the axial stress varies between 2,606 and 6,193 kPa. The variation of radial stress inside the specimen is between 699 and 2,460 kPa.

Although the effect of end restraint decreases with increasing distance away from the end platens, according to Figs. 9 and 10 stresses and strains are highly nonuniform even in the mid-region of the specimen. During the triaxial tests carried out by Anagnostopoulos et al. (1991) for intact Corinth Canal Marl, bulging of the samples was observed. According to the numerical study, it can be seen that the bulging can be due to inhomogeneities and it can develop highly nonuniform stress and strain distributions inside the triaxial specimen. Care should be taken when developing

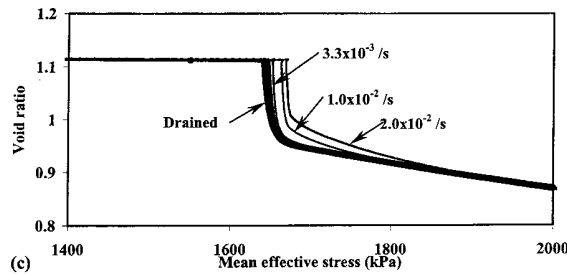
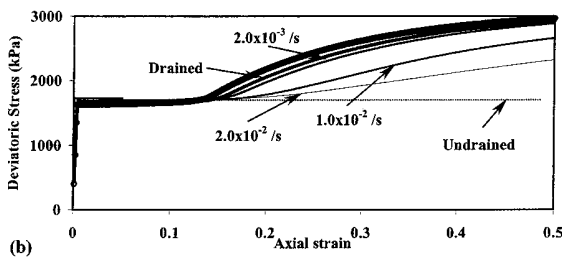
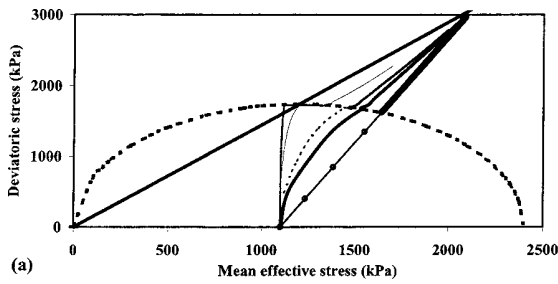


Fig. 11. (a) Stress paths obtained at point A—drainage allowed from all faces; (b) variation of deviatoric stress with axial strain—drainage allowed from all faces; and (c) variation of void ratio with mean effective stress—drainage allowed from all faces

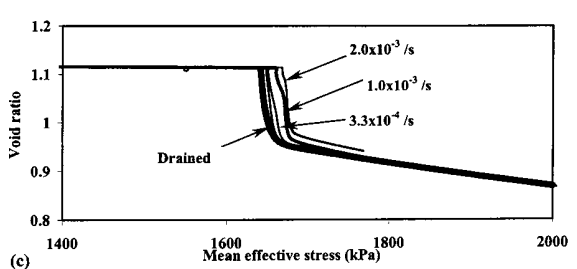
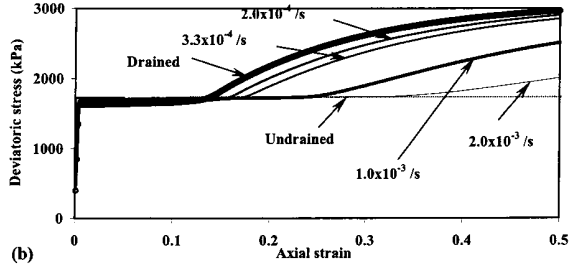
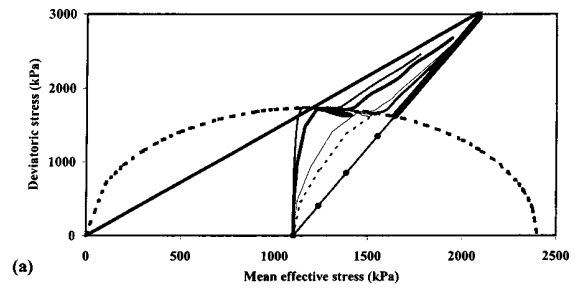


Fig. 12. (a) Stress paths obtained at point A—drainage allowed from top and bottom; (b) variation of deviatoric stress with axial strain—drainage allowed from top and bottom; and (c) variation of void ratio with mean effective stress—drainage allowed from top and bottom

new constitutive relations to make allowance for such experimental behavior.

Effects of Strain Rate

To study the inhomogeneities caused by insufficient drainage during triaxial tests, which were supposed to be fully drained, numerical simulations were carried out using Natural Calcarene specimens. The same amount of axial strain has been applied to the specimens during different time periods, i.e., at different strain rates. In these analyses it has been assumed that the contact between the specimen and the end platens is perfectly smooth, and the rate of axial displacement has been varied.

According to the particle size distribution curve given by Lagioia and Nova (1995), Natural Calcarene is a cemented sandy soil with particle size ranging between 0.1 and 1 mm. Therefore it is assumed that the permeability of the natural calcarenite is $1 \times 10^{-8} \text{ ms}^{-1}$, a typical value for such soils. Fig. 11(a) shows the effective stress paths taken by Point A (Fig. 1) corresponding to different strain rates when drainage is permitted from all faces of the specimen, while Fig. 12(a) shows the corresponding paths when drainage is permitted only from the top and bottom of the

specimen. It is interesting to see that with the increase in the strain rate, the stress path at Point A, which represents the behavior at the center of the triaxial specimen, changes from drained to undrained behavior. Although initially the soil behavior at Point A is either fully drained, undrained, or at an intermediate state depending on the strain rate, after destructuring, it approaches fully drained behavior with increases in both mean effective and deviatoric stresses. Finally, all stress paths at Point A meet the critical state line at the same point as the completely drained case.

Figs. 11(b) and 12(b) show the variation of deviatoric stress with the axial strain based on the global measures, which are comparable with laboratory measurements for the case with drainage permitted from all faces and drainage permitted only from the top and bottom of the specimen, respectively. The fully drained and undrained cases are also shown in these figures. It can be seen that the deviatoric stress at which yielding or destructuring starts is nearly the same for all strain rates and destructuring continues without changing the stress state of the soil. After destructuring, the deviatoric stress variation obtained with different strain rates lies between those obtained from the fully drained and undrained cases. For the cases with drainage allowed from all faces and drainage allowed only at the top and bottom of the specimen, the deviatoric stress reaches the undrained response when the strain rates are 2.0×10^{-2} and $2.0 \times 10^{-3} \text{ s}^{-1}$, respectively, and reaches the drained response when strain rates are

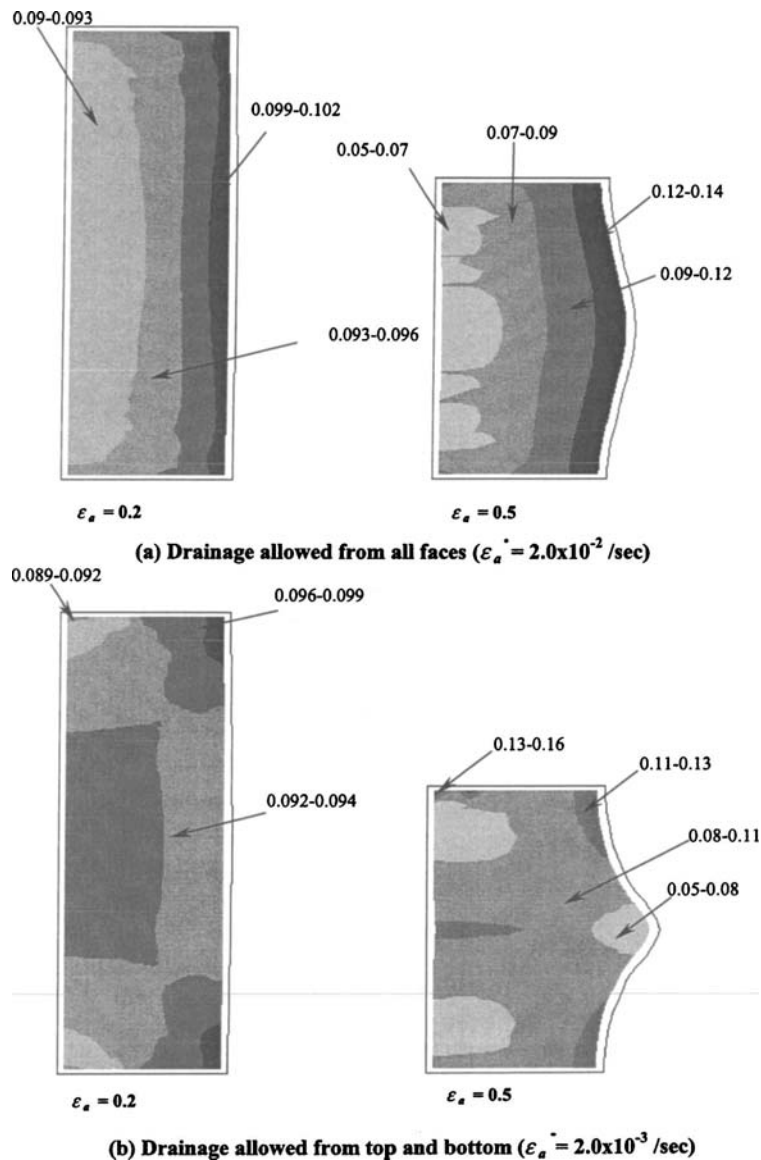


Fig. 13. Volumetric strain distribution inside specimen (Natural Calcarenite)

2.0×10^{-3} and $2.0 \times 10^{-4} \text{ s}^{-1}$, respectively. Hence, if the drainage is allowed from all faces, a strain rate, which is about ten times higher than that used for the case with drainage, allowed only at the top and bottom of the specimen, can be used to obtain fully drained behavior. It is noted however, that Atkinson et al. (1985) and others have shown that the use of radial drainage to speed up drained tests can lead to inhomogeneity of the specimen during isotropic consolidation where the cell pressure is applied incrementally.

Figs. 11(c) and 12(c) show the variation of the globally measured voids ratio with mean effective stress. It can be seen that with the increase in strain rate, the change in voids ratio during the destructuring process reduces but the mean effective stress at which destructuring begins increases.

Although the center of the specimen, i.e., Point A, shows undrained behavior when the strain rate is high, the behavior is not uniform throughout the sample. Figs. 13(a and b) show the volumetric strain inside the specimen when the applied axial strain is 0.2 and 0.5. If the whole specimen behaves as undrained, then the

volumetric strain should be zero inside the specimen. When drainage is allowed from all faces, the volumetric strain varies between 0.04 and 0.14 inside the specimen. If the drainage is allowed only at the top and bottom of the specimen, it varies between 0.05 and 0.16. It can be seen that the deformation of the specimen is also not uniform with the increase in strain rate applied to the specimen. Carter (1982) also showed this by simulating triaxial tests using a finite element model based on the Modified Cam Clay model. This happens due to the nonuniform pore pressure distribution inside the specimen, as shown in Figs. 14(a and b). In both figures, at both axial strain levels considered, it can be seen that near the drainage boundaries soil consolidates and behaves in a fully drained manner. When the strain rate is high, soil behaves undrained in the middle of the specimen and pore pressures build up as the shearing continues. Therefore, the soil is weaker in the middle than adjacent to the drainage boundaries and, despite the smooth ends, the specimen starts to bulge at the mid-region, as can be seen in Figs. 14(a and b).

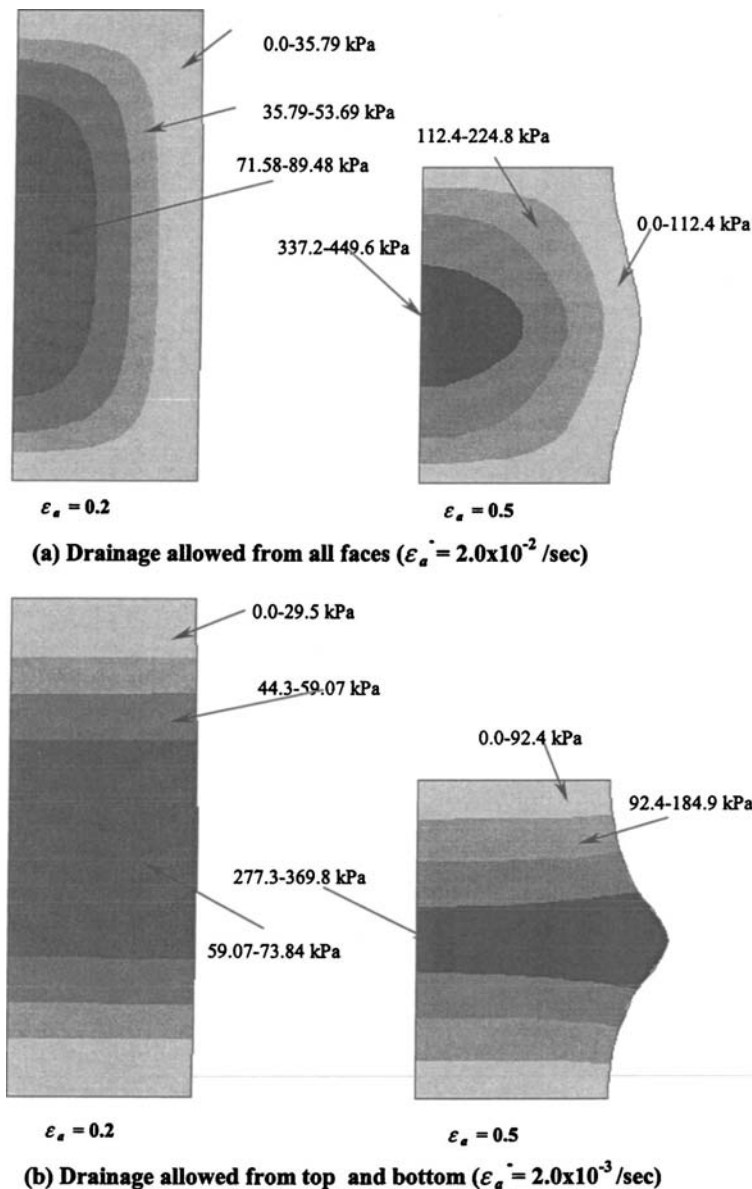


Fig. 14. Pore pressure distribution inside specimen when total axial strain applied to specimen is 0.2 and 0.5

Conclusions

The nonhomogeneous behavior of structured soils in triaxial tests has been studied using a finite element model based on the Structured Cam Clay model incorporating Biot-type consolidation. In order to study the effect of end restraint on the nonhomogeneous behavior of the triaxial specimen, results obtained for an ideal case, where there is no friction between the triaxial specimen and the end platens, have been compared with the case where no movement is allowed between the specimen and the end platens. It could be seen that the destructuring phase of the structured soil has not been influenced significantly by the end restraint but after destructuring, during hardening, the stress-strain behavior of the soil is significantly influenced by the end restraint. Also, it was found that the presence of soil structure will increase the inhomogeneities caused by the end restraint.

Both end restraint and insufficient drainage can cause bulging of the specimen between the end platens. If the drainage is al-

lowed in the radial direction, in addition to the vertical drainage allowed at the top and bottom of the specimen, drained tests can be carried out at strain rates about ten times higher than those required when the drainage is allowed only in the vertical direction at the top and bottom of the specimen. At higher strain rates, soil away from the drainage boundaries behaves in an undrained manner while the soil adjacent to the drainage boundaries is fully drained. With the increase in strain rate, the change in voids ratio during the destructuring phase reduces, but the mean effective stress at which the destructuring commences increases. The stress-strain behavior of soil calculated based on global stress measures comparable with laboratory measurements does not represent the behavior of the soil inside the triaxial specimen after commencement of plastic deformations. This is because the global stresses and strains are affected by the deformation pattern of the triaxial specimen as well as by the constitutive law of the material inside the triaxial specimen, i.e., the specimen exhibits

multielement behavior rather than acting as a uniform single element.

Acknowledgments

This project is part of a project on "Characterisation and Modelling of Structured Soils" funded by the Australian Research Council and has been carried out within the Centre for Geotechnical Research at the University of Sydney. This support is gratefully acknowledged.

References

- Airey, D. W. (1991). "Finite element analyses of triaxial tests with different end and drainage conditions." *Proc., 7th Int. Conf. on Computer Methods and Advances in Geomechanics*, G. Beer, J. R. Booker, and J. P. Carter, eds., Vol. 1, Balkema, Rotterdam, The Netherlands, 225–230.
- Anagnostopoulos, A. G., Kalteziotis, N., Tsiambaos, G. K., and Kavvas, M. (1991). "Geotechnical properties of the corinth canal marls." *Geotech. Geologic. Eng.*, 9, 1–26.
- Atkinson, J. H., Evans, J. S., and Ho, E. W. L. (1985). "Non-uniformity of triaxial samples due to consolidation with radial drainage." *Geotechnique*, 35(3), 353–356.
- Balasubramaniam, A. S. (1976). "Local strains and displacement patterns in triaxial specimens of a saturated clay." *Soils Found.*, 16(1), 101–114.
- Balla, A. (1960). "Stress conditions in triaxial compression." *J. Soil Mech. Found. Div.*, 86(6), 57–84.
- Bishop, A. W., and Green, G. E. (1965). "The influence of end restraint on the compression strength of a cohesionless soil." *Geotechnique*, 15, 243–266.
- Carter, J. P. (1982). "Predictions of the non-homogeneous behaviour of clay in the triaxial test." *Geotechnique*, 32, 55–58.
- Carter, J. P., and Balaam, N. P. (1995). *AFENA user manual, Version 6*, Centre for Geotechnical Research, Univ. of Sydney, Sydney, Australia.
- Duncan, J. M., and Dunlop, P. (1968). "The significance of cap and base restraint." *J. Soil Mech. Found. Div.*, 94(1), 271–290.
- Gens, A., and Nova, R. (1993). "Conceptual bases for a constitutive model for bonded soils and weak rocks." *Proc., Int. Symp. on Geotechnical Engineering of Hard Soils—Soft Rocks*, Anagnostopoulos et al., eds., Balkema, Rotterdam, The Netherlands, 485–494.
- Gens, A., and Potts, D. M. (1988). "Critical state models in computational geomechanics." *Eng. Comput.*, 5(3), 178–197.
- Kavvas, M., and Amorosi, A. (2000). "A constitutive model for structured soils." *Geotechnique*, 50(3), 263–273.
- King, R., and Lodge, M. (1988). "North West shelf development—The foundation engineering challenge." *Proc., Int. Conf. on Calcareous Sediments*, R. J. Jewell and D. C. Andrews, eds., Balkema, Rotterdam, The Netherlands, Vol. 2, 333–342.
- Lade, P. V. (1982). "Localisation effects in triaxial tests on sand." *Proc., Int. Union of Theoretical and Applied Mechanics Symp. on Deformation and Failure of Granular Materials*, P. A. Vermeer and H. J. Luger, eds., Balkema, Rotterdam, The Netherlands, 461–472.
- Lagioia, R., and Nova, R. (1995). "An experimental and theoretical study of the behaviour of a calcarenite in triaxial compression." *Geotechnique*, 45(4), 633–648.
- Lee, K. L. (1978). "End restraint effects on undrained static triaxial strength of sand." *J. Geotech. Eng. Div., Am. Soc. Civ. Eng.*, 104(4), 687–704.
- Leroueil, S., and Vaughan, P. R. (1999). "The general and congruent effects of structure in natural soils and weak rocks." *Geotechnique*, 40(3), 467–488.
- Liu, M. D., and Carter, J. P. (2002). "A structured cam clay model." *Can. Geotech. J.*, 39(6), 1313–1332.
- Locat, J., and Lefebvre, G. (1985). "The compressibility and sensitivity of an artificially sedimented clay soil: The Grande-Baleine Marine Clay, Quebec." *Mar. Geotech.*, 6(1), 1–27.
- Mesri, G., Rokhsar, A., and Bohor, B. F. (1975). "Composition and compressibility of typical samples of Mexico City clay." *Geotechnique*, 25(3), 527–554.
- Mitchell, J. K., and Solymar, Z. V. (1984). "Time-dependent strength gain in freshly deposited or densified sand." *J. Geotech. Eng. Div., Am. Soc. Civ. Eng.*, 110(11), 1559–1576.
- Potts, D. M., Jones, M. E., and Berget, O. P. (1988). "Subsidence above the Ekofisk Oil Reservoirs." *Proc., 5th Int. Conf. on the Behaviour of Offshore Structures*, Vol. 1, Trondheim, 113–127.
- Roscoe, K. H., and Burland, J. B. (1968). "On the generalised stress-strain behaviour of wet clay." *Engineering plasticity*, J. Heyman and F. A. Leckie, eds., Cambridge Univ. Press, Cambridge, U.K., 535–609.
- Rouainia, M., and Muir Wood, D. (2000). "A kinematic hardening model for natural clays with loss of structure." *Geotechnique*, 50(2), 153–164.
- Saada, A. S., and Townsend, F. C. (1981). "Laboratory strength testing of soils, state of the art." *Laboratory Shear Strength of Soil, ASTM Special Publication 740*, R. N. Yong and F. C. Townsend, eds., ASTM, Philadelphia, 7–77.
- Schanz, T., and Gussman, P. (1994). "The influence of geometry and end restraint on the strength in triaxial compression in numerical simulation." *Proc., Int. Conf. on Numerical Methods in Geotechnical Engineering*, I. M. Smith, ed., Balkema, Rotterdam, The Netherlands, 129–133.
- Sheng, D., Westerberg, B., Mattsson, H., and Axelsson, K. (1997). "Effects of end restraint and strain rate in triaxial tests." *Comput. Geotech.*, 21(3), 163–182.
- Small, J. C., Booker, J. R., and Davis, E. H. (1976). "Elasto-plastic consolidation of soil." *Int. J. Solids Struct.*, 12, 431–448.
- Wheeler, S. J. (1997). "A rotational hardening elasto-plastic model for clays." *Proc., 14th Int. Conf. on Soil Mechanics and Foundation Engineering*, Balkema, Rotterdam, The Netherlands, Vol. 1, 431–434.
- Whittle, A. J. (1993). "Evaluation of a constitutive model for overconsolidated clays." *Geotechnique*, 43(2), 289–314.